THE JOURNAL OF BIOLOGICAL CHEMISTRY VOL. 288, NO. 36, pp. 26290–26299, September 6, 2013

Structural Characterization of the Bacteriophage T7 Tail Machinery*◆

Received for publication, June 5, 2013, and in revised form, July 19, 2013 Published, JBC Papers in Press, July 24, 2013, DOI 10.1074/jbc.M113.491209

Ana Cuervo[‡], Mar Pulido-Cid[‡], Mónica Chagoyen[§], Rocío Arranz[‡], Verónica A. González-García[‡], Carmela Garcia-Doval[‡], José R. Castón[‡], José M. Valpuesta[‡], Mark J. van Raaij[‡], Jaime Martín-Benito[‡], and José L. Carrascosa[‡¶1]

From the [‡]Structure of Macromolecules and [§]Systems Biology Departments, Centro Nacional de Biotecnología, Consejo Superior de Investigaciones Científicas, Darwin 3 and the [¶]Instituto Madrileño de Estudios Avanzados en Nanociencia, Cantoblanco, 28049 Madrid, Spain

Background: T7 tail is involved in host recognition, DNA securing, and delivery.
Results: The tail is formed by a tubular structure (proteins gp11 and gp12) surrounded by six fibers.
Conclusion: gp11 is a gatekeeper-adaptor protein, and gp12 closes the ejection channel.
Significance: Tailed bacteriophages may share a common molecular mechanism to coordinate the switch between DNA packaging and tail assembly.

Most bacterial viruses need a specialized machinery, called "tail," to inject their genomes inside the bacterial cytoplasm without disrupting the cellular integrity. Bacteriophage T7 is a well characterized member of the Podoviridae family infecting *Escherichia coli*, and it has a short noncontractile tail that assembles sequentially on the viral head after DNA packaging. The T7 tail is a complex of around 2.7 MDa composed of at least four proteins as follows: the connector (gene product 8, gp8), the tail tubular proteins gp11 and gp12, and the fibers (gp17). Using cryo-electron microscopy and single particle image reconstruction techniques, we have determined the precise topology of the tail proteins by comparing the structure of the T7 tail extracted from viruses and a complex formed by recombinant gp8, gp11, and gp12 proteins. Furthermore, the order of assembly of the structural components within the complex was deduced from interaction assays with cloned and purified tail proteins. The existence of common folds among similar tail proteins allowed us to obtain pseudo-atomic threaded models of gp8 (connector) and gp11 (gatekeeper) proteins, which were docked into the corresponding cryo-EM volumes of the tail complex. This pseudo-atomic model of the connector-gatekeeper interaction revealed the existence of a common molecular architecture among viruses belonging to the three tailed bacteriophage families, strongly suggesting that a common molecular mechanism has been favored during evolution to coordinate the transition between DNA packaging and tail assembly.

Double-stranded DNA (dsDNA) bacteriophages actively package their genetic material inside the capsid using a protein motor that hydrolyzes ATP as an energy source (1). DNA enters the viral head through a channel formed by a protein named connector that sits at a unique 5-fold vertex of the icosahedral capsid (2), a vertex that is also involved in the delivery of the genome during DNA ejection. The ordered packaged DNA generates a high pressure inside the viral head requiring the presence of protein complexes helping to retain the nucleic acid inside the capsid, probably by closing and/or securing the connector channel. In most of the dsDNA viruses, this task is accomplished by a protein or proteins that form a complex that builds a plug at the end of the portal channel, the so-called gatekeeper (3). These proteins also play an important role during the transition between final DNA packaging steps and the subsequent assembly of the tail proteins (3). The tail is a protein complex present in the majority of bacteriophages, which is involved in host recognition and genome delivery. Three main morphologies have been described in tailed phages as follows: short and long noncontractile or long contractile corresponding to Podoviridae, Siphoviridae, and Myoviridae families, respectively (4). Although there is a necessary adaptation of the tail structure of the virus to each viral host family (5), two main features are shared by tail structures; they have a central tubular structure that forms the channel for DNA ejection, which is surrounded by fibers or spikes that are essential in the initial steps of host recognition (5).

The Podoviridae family constitutes the group with the simplest tail morphology, composed of a small number of proteins (6). Structural analysis of different viruses belonging to this group (ϕ29 (7), P22 (8), P-SPP7 (9), N4 (10), ϵ15 (11), and K1E and K1–5 (12)) has shown that these structures are formed by a central knob or nozzle contoured by 6–12 trimeric appendages named fibers or spikes. The tail is attached to the head through the tail adaptor protein, a dodecameric ring with similarities to the gatekeeper proteins described for long-tailed phages (13). The short length of the Podoviridae requires additional components to drill through the whole bacterial envelope, and it has

* This work was supported by Grants BFU2011-29038 (to J. L. C.), BFU2011-25090 (to J. M.-B.), BFU2011-24843 (to M. J. v. R.), and BFU2011-25902 (to J. R. C.) from the Ministry of Economy and Competitiveness.
◆ This article was selected as a Paper of the Week.
The atomic coordinates and structure factors (codes 3j4A and 3j4B) have been deposited in the Protein Data Bank (http://wwpdb.org/).
The three-dimensional EM volumes have been deposited in the EM Data Base (http://www.ebi.ac.uk/pdbe/emdb/) with accession numbers EMD-5689, EMD-5690, and EMD-5713.
[1] To whom correspondence should be addressed: Centro Nacional de Biotecnología, CSIC. %Darwin 3, Cantoblanco, 28049 Madrid, Spain. Tel.: 34-915854509; Fax: 34-915854506; E-mail: jlcarras@cnb.csic.es.

been proposed to be enlarged by internal capsid proteins, which would be also ejected during infection (6, 14). This hypothesis has been recently supported by a cryo-electron tomography study, which has defined for the first time a detailed description of the sequential steps involved in the interaction of the bacteriophage T7 with *Escherichia coli* (15). The bacteriophage T7 infects bacteria by interaction of the tail with one or more bacterial receptors, followed by DNA ejection, and accompanied by extensive structural remodeling of the tail structure (15). Nevertheless, the limited resolution of previous studies from complete viral particles (16, 17) has not yet identified the location and precise topology of the different proteins that constitute the tail structure. Biochemical studies have proposed that the T7 tail machine is formed by proteins gp7.3 (10 kDa), gp8 (59 kDa), gp11 (22 kDa), gp12 (89 kDa), and gp17 (61 kDa) (14). The best structurally characterized proteins are the connector (gp8) and the fibers (built by protein gp17). Purified gp8 protein has been shown to assemble as a dodecamer (18), and gp17 has been shown to assemble into trimers to form the T7 fibers (19–21). Proteins gp11 and gp12 have been proposed to form the central tubular structure of the tail, but their precise location remains unclear (14). Finally, 32 subunits of the protein gp7.3 have been predicted as a component of the tail, but its location and function are controversial. This protein might be involved either in helping the tail protein assembly process or as a part of the tail channel or tip, thus contributing to the host cell interaction (6, 14), and it has also been proposed to be injected inside the bacteria during infection (14).

The biochemical and structural studies carried out in this work have permitted us to define the location and oligomeric state of each of the proteins that form the tail of bacteriophage T7 and to understand their sequential assembly order into the mature DNA-filled viral heads.

EXPERIMENTAL PROCEDURES

Protein Cloning—The genes *11* and *12* from T7 bacteriophage were amplified together or individually by polymerase chain reaction (PCR) using forward and reverse primers containing the BglII-NcoI restriction sites, respectively, with the Expand Long Template PCR System (Roche Applied Science). The fragments were then cloned into the pRSET-B plasmid (Invitrogen) using T4 ligase (Roche Applied Science) overnight at 16 °C. The T7 gene *8* was amplified using the same system with the primers containing the EcoRI-HindIII restriction sites, and it was then cloned into the pRSET-B plasmid containing the T7 *11* and *12* genes. The gene *17*, coding for the fiber protein, was amplified by PCR using forward and reverse primers containing NcoI and HindIII restriction sites, respectively, and cloned into the plasmid pCR2.1-TOPO using topoisomerase I from vaccinia virus (TOPO TA cloning kit, Invitrogen). The fragment coding for the gp17 fiber gene was excised using the aforementioned restriction enzymes and cloned into the expression vector pETDuet (Novagen, Merck Millipore) using the same sites.

Protein Purification—Bacteriophage T7 was produced as described previously (22). Briefly *E. coli* BL21 strain was infected with wild type phage, and the lysate was purified in a cesium chloride step gradient (23) and dialyzed using VISKING dialysis tubing (SERVA) on 50 mM Tris, pH 7.8, 10 mM $MgCl_2$, and 100 mM NaCl (TMS buffer). The tail complexes were obtained by incubating the T7 viruses in the presence of 100 mM EDTA and complete antiproteases mixture (Roche Applied Science) for 45 min at 65 °C. The complexes were complemented with 20 mM $MgCl_2$, incubated with 10 μg/ml DNase (Sigma) for 30 min at 37 °C, and pelleted by ultracentrifugation at 213,000 × *g* for 3 h. The complexes were resuspended in TMS buffer, loaded onto a 10–40% sucrose gradient, and centrifuged at 148,000 × *g* for 105 min. The enriched fractions were concentrated using Amicon ultracentrifugal filter units (Millipore) and loaded onto a Superose 6 10/300 GL column for size exclusion chromatography (GE Healthcare). The sample purity was checked by SDS-PAGE as described previously (14).

The plasmid coding for the gp8, gp11, and gp12 proteins (8-11-12 complex) was transformed into the *E. coli* C41 strain. The culture was grown at 37 °C to an absorbance of 0.6 measured at 600 nm (A_{600}), and then protein expression was induced with 1 mM isopropyl 1-thio-β-D-galactopyranoside for 3 h. The culture was harvested, and the 8-11-12 complexes were found in the supernatant, which was supplemented with complete EDTA-free protease inhibitors (Roche Applied Science) and 1 mM phenylmethylsulfonyl fluoride (PMSF). The complex was precipitated overnight at 4 °C by addition of ammonium sulfate to a final saturation of 40% and pelleted at 6500 × *g* for 1 h. The pellet was resuspended in TMS buffer or 50 mM HEPES, pH 7.5, and 150 mM NaCl containing 10 mM imidazole (no differences were observed between the two buffers). The 8-11-12 complexes, His-tagged at the N-terminal side of gp11 protein, were incubated overnight at 4 °C with Cobalt TALON metal affinity resin (Clontech) and eluted at 1 M imidazole. The enriched eluted fractions were then concentrated on Amicon ultracentrifugal filter units (Millipore) and loaded onto a Superose 6 10/300 GL column as described above. The purity of the samples was checked by SDS-PAGE as described previously (14).

gp8 protein purification was described previously (24). The plasmids coding for gp11 or gp12 were transformed into *E. coli* C41 strain and grown as described above. The cultures were harvested and resuspended into buffer 50 mM Tris, pH 7.8, 500 mM NaCl, 20 mM $MgCl_2$, 2.5 mM β-mercaptoethanol, 10 mM imidazole, with complete EDTA-free protease inhibitor mixture. Cells were lysed by sonication, and the cellular debris was removed by centrifugation at 25,000 × *g* for 15 min. gp12 was precipitated overnight at 4 °C by addition of ammonium sulfate to a final concentration of 40%, pelleted at 25,000 × *g* for 15 min, and resuspended in the same buffer. The N-terminal His-tagged proteins were purified in a TALON affinity resin as described above and eluted at 1 M imidazole. gp11 protein was pure enough after this step; gp12 protein was dialyzed in buffer 50 mM Tris, pH 7.8, 50 mM NaCl, 20 mM $MgCl_2$, and purified into an ion exchange chromatography on a ResourceQ column (GE Healthcare), where the protein was eluted at 250 mM NaCl. The purity of the proteins was checked by SDS-PAGE. To study its oligomerization state, gp11 was loaded into a Superdex 200 10/300 GL (GE Healthcare) column for size exclusion chromatography. Bovine albumin, ovalbumin, anhydric carbonase, and cytochrome *c* were used as protein markers.

In Vitro Fiber Assembly— gp17 fiber protein was produced in *E. coli* strain BL21(DE3). The culture was grown at 37 °C up to an A_{600} between 0.6 and 0.8, induced with 1 mM isopropyl 1-thio-β-D-galactopyranoside, and grown for 16 h at 16 °C. Harvested cells were resuspended in 50 mM Tris-HCl, pH 8.9, 4% glycerol, 50 mM ammonium chloride, 2 mM EDTA, 150 mM sodium chloride and then frozen at −20 °C. The cells were lysed by several freezing and thawing cycles and centrifuged to eliminate cell debris. A one-to-one culture volume ratio of the gp17 extract was mixed with 8-11-12 complexes after the ammonium sulfate precipitation step (see above) and resuspended in 50 mM HEPES, pH 7.5, 150 mM NaCl, and 10 mM imidazole. The mixture was incubated for 1 h at 30 °C and mixed with TALON resin (as described above). The 8-11-12 complexes that have incorporated gp17 protein did not bind to the resin and were eluted during the washes. The sample was then precipitated with ammonium sulfate at 40% saturation, pelleted for 15 min at 25,000 × *g*, and loaded onto a 10–40% sucrose gradient and centrifuged, followed by size exclusion chromatography as described above. gp17 protein was purified following the same protocol.

Pulldown Assays—For production of gp8 antibodies, nine BALB/c mice were inoculated in three cycles with 780 μg of purified His-tagged gp8 protein (Protein Tools Unit). Protein G Dynabeads (Novex by Invitrogen) were coated with gp8 antibodies following the manufacturer's instructions. The gp8-gp11 interaction reactions were performed at 1:1 or 1:0.5 μM ratios and incubated for 1 h at 30 °C in TMS buffer. The reactions were then incubated with anti-gp8-coated beads and washed following the manufacturer's instructions. The bound complexes were boiled at 99 °C for 5 min, analyzed by SDS-PAGE, followed by Western blotting, incubated with anti-His antibody (Sigma), and developed with an enhanced chemiluminescence kit (ECL, GE Healthcare).

Electron Microscopy and Image Processing—Electron microscopy of negatively stained samples was performed as described previously (18). gp12 images were acquired on an FEI Tecnai FEG200 electron microscope operated at 200 kV, using low dose protocols with a 4K × 4K Eagle CCD camera (Gatan Inc.) at a nominal magnification of ×108,696 and a defocus range of 1.5–3.5 μm. The contrast transfer function was corrected in the micrographs using standard XMIPP software (25); the particles were manually selected with XMIPP (26) and down-sampled to a factor of 3 to a final pixel size ratio of 4.14 Å/pixel. Images were classified using XMIPP reference-free clustering approach classification methods (CL2D) (27), and 640 particles corresponding to side views were selected. A Gaussian blob was used as a starting model to perform a three-dimensional reconstruction using a restricted projection angle protocol with EMAN (28). Next the model was refined using XMIPP Projection Matching package (25). For cryo-electron microscopy, the samples were applied to Quantifoil 2-μm holey carbon grids coated with a thin carbon layer, frozen in liquid ethane, and transferred to a FEI Tecnai FEG200 operated as described above. Tail complex images were acquired at a nominal magnification of ×50,000, and the selected micrographs were scanned on a Zeiss scanner (Zeiss SCAI scanner) with a step size of 7 μm. The images of the 8-11-12 complexes were acquired under the same conditions but using a 4K × 4K Eagle CCD camera at a nominal magnification of ×108,696. Next, images were contrast transfer function-corrected (25) and down-sampled by a factor of 2 to a final pixel size ratio of 2.8 and 2.75 Å/pixel for the tail and the 8-11-12 complex, respectively. To perform the three-dimensional reconstructions, 3056 and 1820 particles of the tail and the 8-11-12 complex, respectively, were extracted, normalized, and two-dimensionally aligned and classified using reference-free XMIPP maximum likelihood (ML2D) (29) and CL2D (27) procedures. Averages resulting from these classifications were used to generate an initial three-dimensional model based on the common line methods implemented in the EMAN software (28) applying 6-fold symmetry. These initial models were refined using SPIDER (30) or XMIPP Projection Matching package (25). The final resolutions using the 0.3 Fourier shell correlation criterion were ~16 Å for the tail complex and ~12 Å for the 8-11-12 complex. Three-dimensional volumes and images were generated with the University of California at San Francisco Chimera software (31).

Structural Modeling (Threading), Segmentation, and Fitting—Appropriate templates for model building of portal protein gp8 were found with HHpred (32). These corresponded to the enterobacteriophage P22 connector protein (*E*-value 5.5*E*-05, *p* value 2*E*-09, 10% identity) and the bacteriophage SPP1 portal protein (*E*-value 0.18, *p* value 5.4*E*-10, 12% identity). The final structural model of gp8 was built with I-TASSER (33), using the fully automatic procedure. Alignment of gp8 with P22 connector protein was produced by I-TASSER. Structural templates for gp11 were assessed with several sequence-based and threading algorithms providing no significant output. In the absence of a clear template for gp11, a sequence profile was created and further used to search against the InterPro database (34) using HHpred (32). The first two hits corresponded to Pfam domains of unknown function, and the third to Pfam P22 tail accessory factor (PF11650). None of these hits were statistically significant. Nevertheless, functional and structural data indicated that T7 gp11 and P22 gp4 have similar roles. Therefore, a structural model for gp11 was built using the atomic structure of gp4 from enterobacteria phage P22 (PDB code 1vt0 chain k). The sequence alignment provided by HHpred was used to guide the I-TASSER modeling (33). Segmentation of gp8 and gp11 oligomers was carried out manually using the University of California at San Francisco Chimera software (31). A 12-fold symmetry was imposed to the maps using proc3d EMAN package (28). The monomer models were manually fitted as rigid bodies into the EM electron density using Chimera, and the oligomers were built using pdbsymm program from the SITUS package (35). Atomic structures were presented using PyMOL (Delano Scientific LLC, San Francisco) and EM maps using Chimera (31).

RESULTS

Structure and Protein Composition of the T7 Tail Complex—T7 virions incubated with 100 mM EDTA results in the disruption of the viral particles into separate heads and tails (data not shown). The tail complexes, purified by sucrose gradient centrifugation and size exclusion chromatography, consist of the connector protein (gp8) and the tail proteins gp11, gp12, and

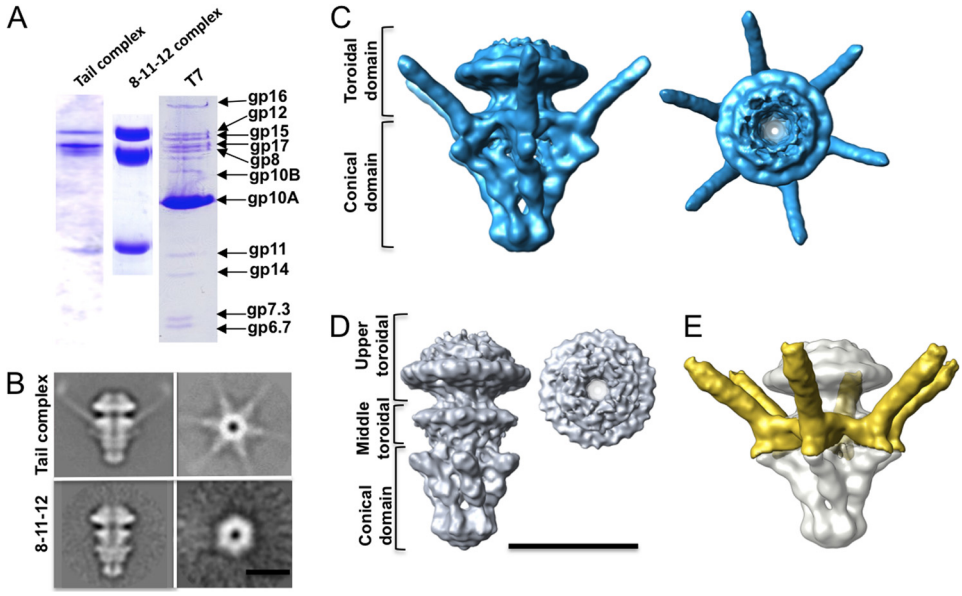

FIGURE 1. **Structural and biochemical characterization of T7 tail complexes.** *A,* Coomassie-stained SDS-PAGE showing the proteins present in the phage-extracted tail complex, the recombinant 8-11-12 complex, and the complete T7 phage particle. The position of the T7 proteins is marked with an *arrow*. *B,* two-dimensional averages of electron microscopy images showing side (*left panel*) and end-on views (*right panel*) of the extracted tail complexes (*top panel*) and recombinant 8-11-12 complexes (*bottom panel*). *C,* three-dimensional volume of the phage-extracted tail complex in side (*left panel*) and end-on (*right panel*) views. *D,* three-dimensional volume of the 8-11-12 complexes showing side and end-on views, (*left* and *right panels*, respectively). *E,* side view of the difference map of the three-dimensional volumes described in *C* and *D*. The reference volume is shown in *contour lines*. The *scale bar* is 20 nm.

gp17 (Fig. 1*A*). Protein gp7.3 was not detected in any of our tail complex purifications. Cryo-EM of the vitrified tail complexes (Fig. 1*B*) showed images that, after two-dimensional averaging, revealed projections characteristic of side views of the tails as follows: a 29-nm-long tubular structure with a central channel that is closed at the narrower end (Fig. 1*B, upper row, left panel*). The averaged projections corresponding to the end-on view of the tail complex clearly shows the existence of six fibers, radially extending, which are better defined in the domain proximal to the tail axis (Fig. 1*B, upper row, right panel*). Three-dimensional reconstruction (3DR)[2] from the vitrified tail complexes using single particle image reconstruction methods produced a volume showing a roughly conical structure with two well defined morphological domains along the longitudinal axis (Fig. 1*C*). The upper domain is a toroidal region with a clear 12-fold symmetry, which showed an overall similarity to other viral connector structures (2, 18). The lower domain of the complex has a conical shape, with six conspicuous upward pointing fibers, and ends in a closed nozzle structure (Fig. 1, *B* and *C*). This overall structure is very similar to the one described for the tail in the complete phage (15, 16), strongly suggesting that the complex has not suffered detectable structural changes during detachment from the phage. The ~15-nm-long thin fibers are tilted by around 42°, and this topology was similar to the so-called upward conformation described in intact virions from tomographic reconstructions (15). In addition, the overall structure of the T7 tail described here notably resembles the cyanophage P-SPP7 tail (9), also a member of the Podoviridae family. This structural similarity suggests that both viruses may have a common infection mechanism.

To obtain a direct mapping of the different structural proteins in the tail, we cloned and expressed each protein alone or in combination with the others, as block-cloning strategies have been successfully used to obtain other tail components (such as the base plates) in lactococcal phages (36). The joint expression of the genes *8*, *11*, and *12* resulted in the assembly of fiber-less tail complexes, referred to in this study as the 8-11-12 complex. The absence of the flexible fibers facilitated the cryo-electron microscopy data acquisition with respect to the complete tail complex, and it was possible to reconstruct the volume of this fiber-less complex at a resolution of ~12 Å (Fig. 1*D*). Averaged projections of the side and end-on views of the complex revealed a very similar structure with respect to the tail complex (Fig. 1*B*, *lower row*), with identical dimensions and overall shape, and with the channel also closed at the nozzle end. The main difference is located at the level of the fibers protruding from the sides of the main body of the tail. In this case, the absence of the fibers allows us to distinguish a new toroidal region at the intermediate position between the connector, in the upper part, and the conical region, in the lower part. This intermediate structure also shows a clear 12-fold symmetry. Additionally, the higher resolution of this reconstruction permits us to discriminate two regions into the conical domain, one with six protrusions extending outward from the complex axis at an angle similar to the tail fibers and another, at the vertex, defining a nozzle, which serves as the channel closure (Fig. 1*D*). The difference map between the 3DR of the complete tail and the 8-11-12 complex (Fig. 1*E*) revealed that both structures were very similar with the exception of the density that corresponds to the fiber proteins (Fig. 1*E*). As the difference between both complexes resides in the presence of the protein gp17, this protein should build the six well defined fibers. A study of isolated fibers by Steven *et al.* (20) demon-

[2] The abbreviations used are: 3DR, three-dimensional reconstruction; PDB, Protein Data Bank.

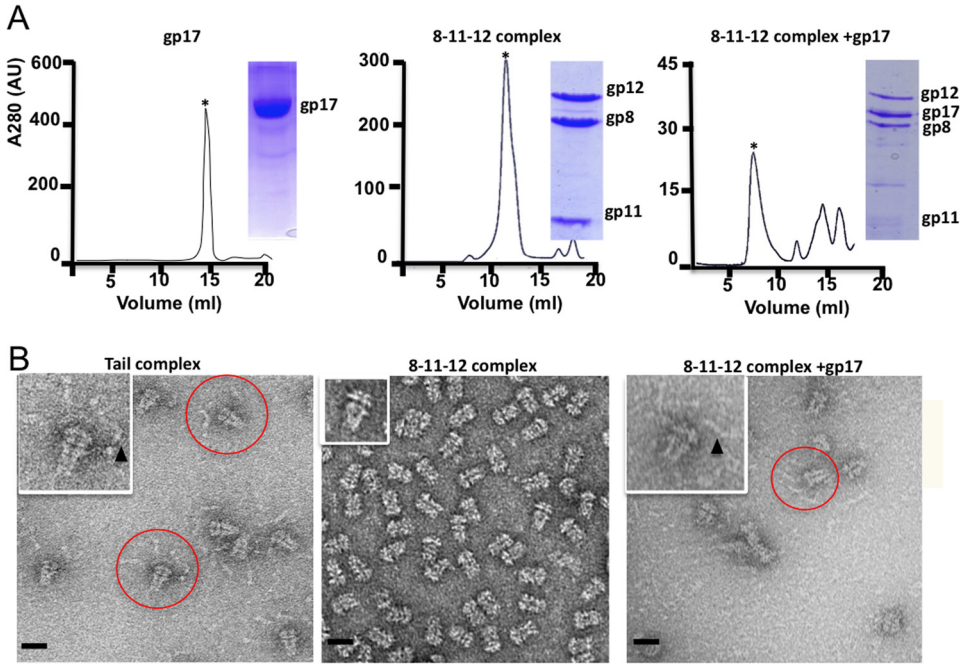

FIGURE 2. ***In vitro* assembly of the fibers.** *A,* chromatograms showing the elution volume of the gp17 trimers (*left panel*), the 8-11-12 complex (*center panel*), and the complex incubated with gp17 (*right panel*). The peak corresponding to each complex is marked with an *asterisk*. The protein content of the peak fraction is characterized in Coomassie-stained SDS-PAGE. *B,* micrographs of negatively stained samples showing the phage-extracted tail complex (*left panel*), the 8-11-12 complex (*middle panel*), and the recombinant 8-11-12 plus gp17 complex assembled *in vitro*. The *bar* represents 30 nm. Representative views of fiber complexes are highlighted with a *red circle*. In the *upper left corner* is shown a zoomed-in complex where the C-terminal end of the fiber is marked with an *arrowhead*.

strated that the gp17 trimer forms a kinked thin fiber 2 nm in diameter and a length of 32 nm. As the length of the fibers we have reconstructed in the tail is around 15 nm, it is clear that this density corresponds to the proximal N-terminal half-fiber (16.4 nm long) described in the isolated gp17 trimer (20). The lack of the distal carboxyl part of gp17 in our assembled fibers is probably due to the flexibility of the fibers around its hinge, which prevents their averaging. This flexibility has been proposed as a critical factor in the structural transitions involved in the phage-bacteria interaction, and their conformation might be stabilized by its interaction with the capsid (15).

Comparison between the tail and the fiber-less models (Fig. 1, *C--E*) allowed us to clearly define the docking point of the fibers in specific positions of the middle and the lower tail domains and to unambiguously identify the composition of these two domains of the tail complexes formed by proteins gp11 and gp12. It has been previously discussed that the protein gp7.3 could be present in the central tail channel or in the tail tip (14), but we have not detected it in any of the complexes described here. Although we cannot exclude that the protein has been lost from the tail during the chemical treatment needed to extract the tail complex from the virion, the structural similarity between the structures characterized here and the one present in the entire phage (15, 16) suggests that gp7.3 protein is not a structural protein of the mature T7 tail.

gp17 Fiber Assembles into the Tubular Tail Complex in Vitro—To study the assembly of the different structural components of the tail complex, we tested whether the 8-11-12 complex was able to incorporate gp17 protein *in vitro*. The extracts containing the 8-11-12 complexes and the extract derived from the separately cloned gp17 were incubated together at 30 °C, purified, and then analyzed for the presence of complexes. Although purified free gp17 trimers and control complexes (not incubated in the presence of gp17) eluted in the size exclusion chromatography column at a volume of 14 and 12 ml, respectively, the complexes assembled in the presence of gp17 eluted at a volume of 8 ml (Fig. 2*A*). This difference in elution volume suggested an increase in the size of the gp17-incubated complexes. SDS-PAGE of the peak fractions showed the presence of gp17 in the larger complexes (Fig. 2*A*). Analysis by electron microscopy of these samples showed that although no fibers were observed in the control complexes (Fig. 2*B*, *middle panel*), the complexes incubated in the presence of gp17 contained the typical fibers, and they were identical to the ones extracted from the viral particles (Fig. 2*C*, *right* and *left panels*, respectively). These experiments strongly suggested that the His-tagged 8-11-12 complexes present a native structure, as they are able to assemble the fibers. Furthermore, the binding of the gp17 fibers to the pre-assembled tubular 8-11-12 complex suggests that this protein is the last protein to be incorporated into the virus during the morphogenetic pathway. This result matches previous experiments in which fiber-less viruses incorporated fibers using gp17 extracts (14).

Localization of gp11 and gp12 Tail Proteins—Cloning and purification of the isolated gp8, gp11, and gp12 proteins allowed us to carry out biochemical assays to identify the interactions that take place inside the tail complex. Pulldown assays using Dynabeads coated with anti-gp8 antibody allowed us to assign the interaction between gp8 and gp11 proteins (Fig. 3*A*). Although purified gp11 alone was not able to bind to the anti-gp8 antibody-coated beads, a significant amount of this protein interacted with gp8 as seen in the precipitation with the gp8

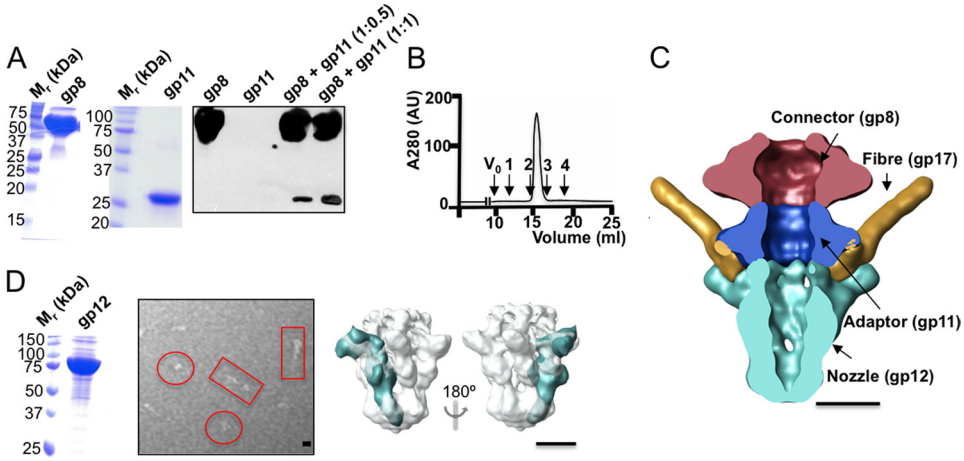

FIGURE 3. **Localization of the tail proteins inside the complex.** *A,* Coomassie-stained SDS-PAGE (*left panel*) showing the purification of connector (gp8) and minor tail (gp11) proteins. Western blot was developed with an anti-His tag antibody showing the pulldown assays used to characterize the gp8-gp11 interaction (*right panel*). *B,* chromatogram showing the elution volume of the gp11-purified protein. The *arrows* show the elution volume of the void volume (V_0) and the protein markers as follows: *1,* bovine albumin (67 kDa); *2,* ovalbumin (43 kDa); *3,* carbonic anhydrase (29 kDa), and *4,* cytochrome *c* (14 kDa). *AU,* absorbance units. *C,* side section of the tail complex structure showing the localization of gp8 (*red*), gp11 (*dark blue*), gp12 (*green*), and gp17 (*orange*) proteins. *D,* Coomassie-stained SDS-PAGE (*left panel*) showing the purification of the major tail protein (gp12). *Middle panel,* micrograph of a negatively stained sample showing a gp12 representative field. Side views and end-on views are marked with a *red square* and *a circle*, respectively. *Right panel,* two different side views of the reconstructed gp12 monomer structure (*green*) docked inside of the gp12 hexamer volume segmented from the 8-11-12 complex structure (*gray contour lines*). The *scale bar,* 4 nm.

antibody (Fig. 3*A*). This interaction clearly identifies the location of gp11 inside the reconstructed tail complex, as forming the 12-fold symmetric toroidal domain immediately below the connector (Fig. 3*C*), an oligomeric state previously proposed for gp11 (14). To study the oligomeric state of gp11 in solution, we performed size exclusion chromatography of the purified protein (Fig. 3*B*). The protein eluted between 43- and 29-kDa protein markers, which clearly suggests that the protein is present as a monomer in solution when it is not interacting with gp8 connector protein. The location of gp11 in the tail, together with its oligomerization change upon assembly (between monomer and dodecamer), strongly suggests that gp11 could be a gatekeeper protein that acts as an adaptor protein. In other phages these proteins also show a monomeric form that acquires a dodecameric architecture after interacting with the connector (3, 13, 37, 38).

The third structural component of the tail tube, gp12, would then form the end of the tail, including the conical tube, the nozzle, and the small extensions below the fibers (Fig. *3C*). The existence of 6-fold symmetry in this domain (previously suggested in Ref. 14) supports a fixed fitting of this domain with the upper gatekeeper. The size of the gp12 protein (89 kDa) allowed its direct observation in the electron microscope (Fig. 3*D, middle panel*). Image processing of negatively stained samples led us to obtain the 3DR of the gp12 protein. The volume presented an elongated shape (around 14 nm long and 4 nm wide), whose structural features are in agreement with the volume of each of the six monomers observed in the conical domain of the tail (Fig. 3*D*, *right panel*). The fitting of the gp12 negatively stained volume in one of the six lobes of the gp12 hexamer segmented from the 8-11-12 cryo-EM map (Fig. 3*D, right panel*) strongly suggests that gp12 is also present as a monomer in solution and that it is its interaction with the gp11 gatekeeper that drives its assembly as a hexameric nozzle containing the tail end.

Protein gp11 Shares Structural Similarities with Adaptor-Gatekeeper Proteins from Other Phages— gp4 from phage P22 and gp11 from phage T7 have similar locations, and therefore both proteins might share structural features. Even though no sequence homology was found between these proteins, protein structure prediction methods suggested that they indeed might have a common fold. The model of the gp11 T7 protein was thus obtained by threading methods using as a template the gp4 protein of P22 (13). The overlay of the gp11 model with the atomic structures of proteins gp4 from P22 and also gp6 from Siphoviridae phage HK97 pointed to the presence of four α-helices preserved in all three structures (Fig. 4*A*) (13, 37). The N-terminal end of the gp11 structure is nevertheless unique, and its atomic structure could not be predicted by the threading. Our results indicated that gp11 would be formed by two different modules as follows: one, which is more conserved with respect to other tailed phages (13, 37, 39, 40), builds the central channel of the gatekeeper structure, and second, another new module that might be involved in the interaction with the fibers for their subsequent binding. The differences between fiber and spike structures presented in T7 and P22 (41), respectively, may explain the modifications in the corresponding folds of the gatekeeper proteins.

The presence of two cysteine residues in the gp11 sequence (*C121* and *C159*, Fig. 4*B*, *left panel*) allowed testing the validity of the threaded gp11 model. According to our proposal, these residues are placed close enough in the folded structure to form a disulfide bond under nonreducing conditions. Gel electrophoresis analysis of purified gp11 in the absence of reducing agent showed the presence of a band migrating faster (gp11-SS) than the reduced gp11 (Fig. 4*B*, *right panel*). This could indicate that an intra-molecular disulfide bond is indeed formed. A similar result was obtained when the protein was assembled inside the 8-11-12 complex, indicating that this disulfide bond was

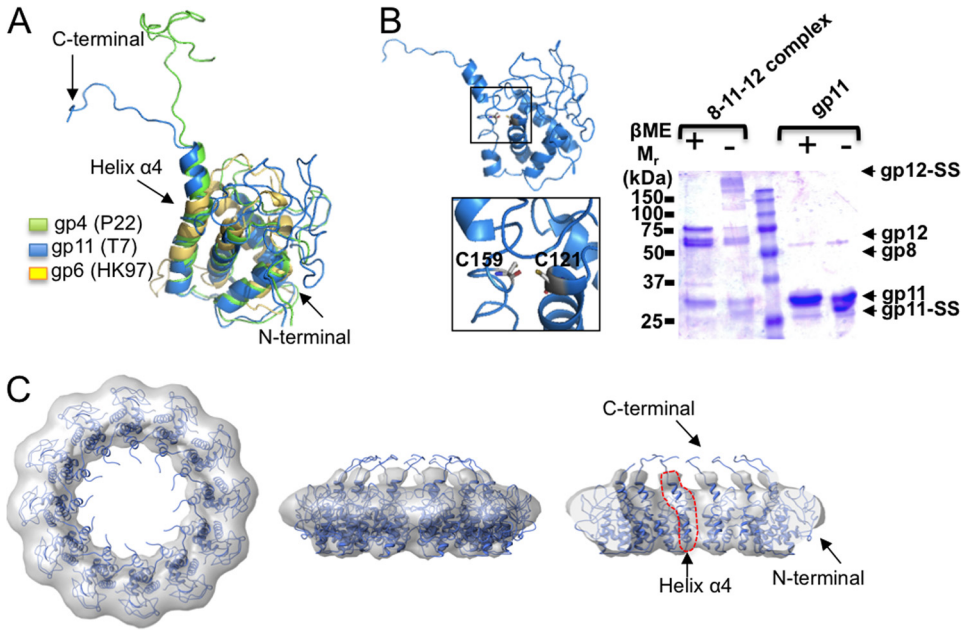

FIGURE 4. **Bacteriophage T7 gp11 protein.** *A, ribbon* representation of the gp11 T7 model overlapped with the atomic structures of the gp4 P22 (PDB code 3LJ4) and gp6 HK97 (PDB code 3JVO). N- and C-terminal ends and α4 helix are marked with *arrows*. *B, ribbon* representation of gp11 showing the position of the cysteine residues Cys-121 and Cys-159. The *square* represents the zoomed-in area (*bottom panel*). Coomassie-stained SDS-PAGE showing the behavior of the proteins of the 8-11-12 complex and gp11 in the presence (+) or absence (−) of the β-mercaptoethanol-reducing agent (*right panel*). The bands corresponding to the gp8, gp11, and gp12 monomers and intra-molecularly disulfide-bonded gp11 (gp11-SS) and inter-molecularly disulfide bonded gp12 (gp12-SS) are marked with *arrowheads*. *C,* docking of the gp11 pseudo-atomic structure inside of the volume segmented from the 8-11-12 complex structure showing an end-on (*left panel*), side (*middle panel*), and side section views (*right panel*). The location of the internal α4 helix is contoured with a *red dashed line* and an *arrow*. The location of the N-terminal and C-terminal ends are marked with *arrows*.

formed when the protein is in its native structure (Fig. 4*B*, *right panel*). In the latter case, a high molecular mass band (gp12-SS, with a relative mass higher than 150 kDa) was also observed when the reducing agent was absent (Fig. 4*B*, *right panel*). The partial disappearance of the gp12 monomer band and the presence of five cysteine residues inside its sequence suggested that this band could correspond to inter-molecular gp12 disulfide cross-linking.

To generate a pseudo-atomic model of the gp11 toroidal complex, the volume corresponding to this protein was segmented out of the 8-11-12 complex structure. Then 12-fold symmetry was imposed to the map, and the threaded gp11 model was docked inside this volume (Fig. 4*C*). The precise docking of the model confirmed that gp11 was present in the phage as a dodecamer, as is the case for gp4 from P22 (13) and gp6 from HK97 (37). The docking shows that the oligomer is assembled in the same way as in P22, with the α4 helix (the most C-terminal of the helices) building the internal surface of the central channel (Fig. 4*C, right panel,* contoured in *red*). The C-terminal domain ends in a long loop that might be implicated in the interaction with the connector (Fig. 4, *B, left panel,* and *C, arrows*). The nonmodeled N-terminal side of the protein is located at the outside part of the ring, and it might form an interaction surface with the fibers.

Protein gp8 Presents an Internal Channel Formed by a 24α-Helix Stretch Characteristic of Connector Proteins—The 3DR of the 8-11-12 complex also allowed us to obtain a detailed model of the structure of the connector (gp8) and its interaction with the gatekeeper (gp11). The model of gp8, containing residues 1–497, was obtained by threading using the P22 connector (gp1) as template (Fig. 5*A*) (13). The threaded model presented the overall structure previously described for other connector proteins (2), composed by the stem, crown, and wing domains (Fig. 5*A*, *right panel*). The superposition of the gp8 model with the atomic structures of p10 from ϕ29 (42, 43), gp1 from P22 (13), and gp6 from SPP1 (44) showed that the topology of the helices that form the internal surface of the channel is conserved among the four structures (Fig. 5*A*, *left panel*). The lower end of these structures, which can be either formed by a helix-β-sheet motif or an unstructured loop, is highly variable. This structural variability is probably related to the multitask activity of this region, which has to interact with the viral ATPase (terminase) in the early steps of the assembly pathway (the terminase is later detached from the complex and replaced by the gatekeeper protein). Another region that showed variability was the C-terminal region, where a group of three helices adopt a more open or close conformation depending on the connector protein. Segmentation of the gp8 volume from the 8-11-12 complex map allowed docking the model inside (Fig. 5*B*). A good fit is observed between the model and the cryo-EM map, confirming the quality of the structural model obtained. The only discrepancy is located at the bottom part (Fig. 5*B*, *middle* and *right panels*), suggesting that this region may have a different conformation in the assembled tail complex for the reasons discussed above. The segmented volume presents some differences with the structure previously described for the isolated connector, notably in the C-terminal domain (crown) (18). This region was found more prominent in the isolated connector dodecamer, suggesting that it might present some structural flexibility when gp8 is assembled in the tail structure.

The fitting of the pseudo-atomic models of gp8 and gp11 inside the 8-11-12 complex 3DR showed that both proteins

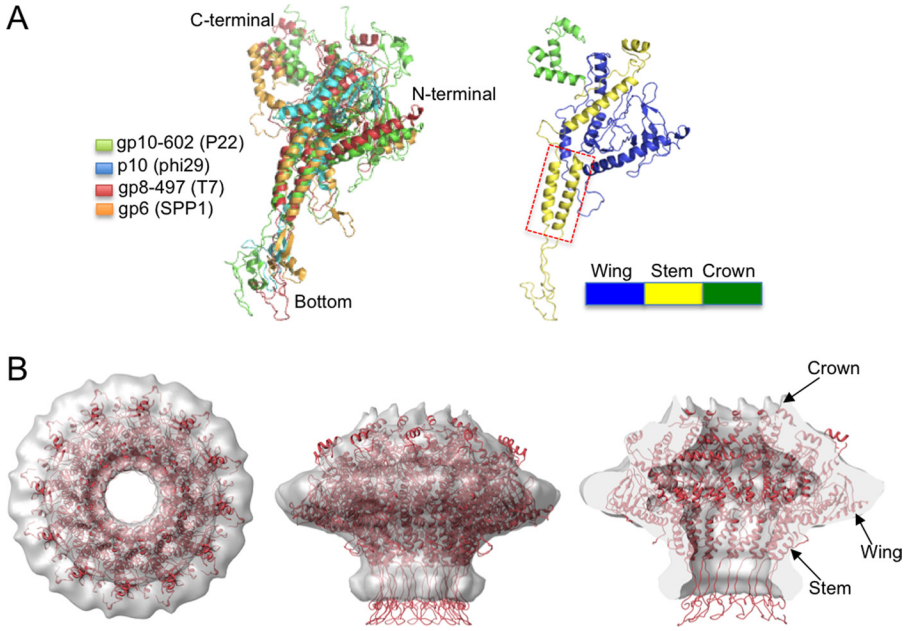

FIGURE 5. **Bacteriophage T7 gp8 connector protein.** *A, ribbon* representation of residues 1–497 of the gp8 model (*left panel*) overlapping with the connector atomic structures of the gp6 SPP1 (PDB code 2JES), residues 1–602 of the gp10 P22 (PDB code 3LJ5), and p10 ϕ29 (PDB code 1H5W). On the *right*, the gp8 1–497 model show the connector domains as follows: wing (*blue*), stem (*yellow*), and crown (*green*). The conserved helices forming the internal channel are marked with a *red dashed line*. *B,* docking of the gp8 pseudo-atomic structure inside of the volume density segmented from the 8-11-12 complex structure in an end-on (*left panel*), side (*middle panel*), and a side section views (*right panel*).

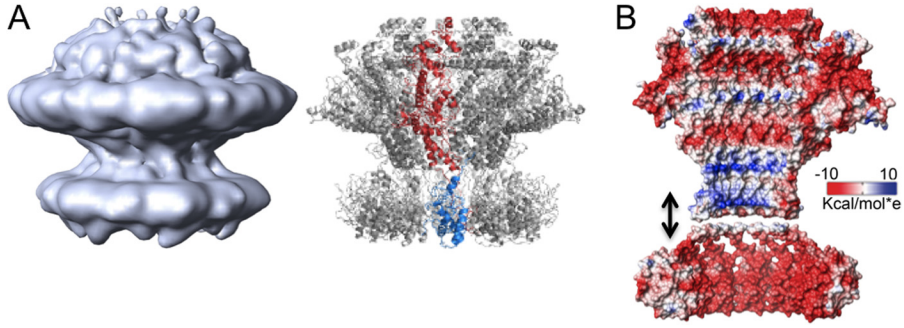

FIGURE 6. **Model of the gp8-gp11 complex.** *A,* volume built from the gp8 and gp11 proteins segmented from the 8-11-12 complex structure (*left panel*). *Right panel,* ribbon representation of the gp8 (residues 1–497) and gp11 pseudo-atomic structures fitted into the 8-11-12 complex structure. A single subunit of the gp8 connector protein is shown in *red* and that of the gp11 protein is shown in *blue*. *B,* electrostatic isosurface of the gp8-gp11 channel inner wall calculated using University of California at San Francisco Chimera software showing six chains of each protein. The color code ranges from *red* (negative) to *blue* (positive).

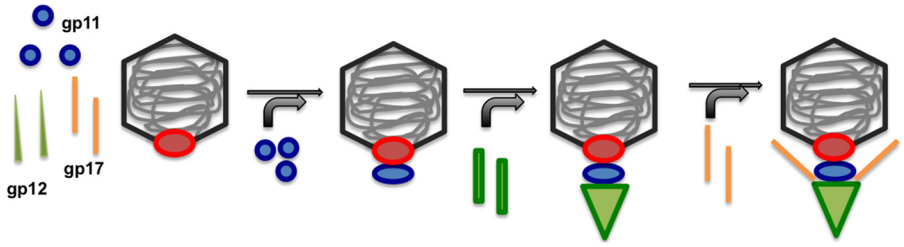

FIGURE 7. **Diagram representation of the T7 tail assembly pathway.** Schematic picture showing the sequential assembly pathway proposed for the tail proteins. gp11 and gp12 monomers are represented in *blue* and *green*, respectively, and gp17 fiber trimers are shown in *orange*. Once the DNA is packaged inside the capsid, gp11 assembles upon binding to the connector (in *red*), and subsequently, gp12 monomers dock to the gatekeeper protein generating the proper environment allowing the interaction of the fiber trimers to build the final mature tail.

present an overall assembly and interaction very similar to the one previously described in P22 (13), with the characteristic helices forming the central channel of the tail assembly (Fig. 6*A*). The electrostatic isosurface of the complex showed that the internal channel presents an overall negative charge (Fig. 6*B*). This highly electronegative environment has also been described for other portal channels as an essential characteristic to avoid DNA interaction with the complex during the packaging and ejection processes (2).

DISCUSSION

Our results reveal the detailed location of gp8, gp11, gp12, and gp17 proteins in the tail of bacteriophage T7 (Fig. 3*C*). The overall architecture of the T7 tail is very similar to the one of

P22 bacteriophage (41), also belonging to the Podoviridae family, composed of a gatekeeper protein that serves as an anchoring point for the rest of the tail components to the viral head. The results presented here show that the folds and interactions between the connector and gatekeeper proteins belonging to both phage types seem to be closely related. Evolutionary studies have clearly shown that structural folds usually diverge slower than amino acid sequences, and thus structural similarity can be used to infer an evolutionary and functional relationship between viruses (40). The structural similarities found between the connector and gatekeeper proteins of T7 and other phages also reinforce the idea that bacteriophages share several key building blocks that have been conserved during evolution. Capsid protein and connector proteins have been well characterized as basic evolutionary keystones for the existence of common mechanisms for building highly efficient DNA-containing particles. The existence of similarities also in gatekeeper proteins belonging to Podoviridae, Siphoviridae, and Myoviridae phage families (5, 40) could suggest that a common molecular mechanism has been favored to carry out the transition among the later steps of viral assembly to synchronize the switch between DNA packaging and tail protein attachment. Our experiments suggest a sequential interaction of the T7 tail proteins during the viral maturation (Fig. 7), revealing that the different monomeric proteins only assemble into the tail complex after the precursor structure generates the proper interaction domains, a mechanism closely related to the one described for bacteriophage P22 (45, 46). In this way, a possible sequence of the final steps in the maturation process could be as follows: after the DNA is fully packaged by the terminase inside the prohead, the connector must undergo a structural change to trigger the release of the terminase. This change, in turn, favors the interaction with monomers of the protein gp11, which will dock to the portal vertex building the dodecameric gatekeeper to secure the DNA inside the mature viral head. This complex subsequently allows the interaction with gp12 and the assembly of six gp12 monomers to form the hexameric tubular end of the tail and the nozzle, to close the DNA ejection channel of the tail. Once the tail tubular structure is formed, the interface between the gp11 and gp12 proteins generates the appropriate structural environment to interact with six gp17 trimers to bind the fibers and to generate the complete tail.

Acknowledgments—We thank the Protein Tools Unit Facility at the CNB for gp8 antibody production. We are indebted to Alina Ionel for previous work on T7 tail complex preparation.

REFERENCES

1. Casjens, S. R. (2011) The DNA-packaging nanomotor of tailed bacteriophages. *Nat. Rev. Microbiol.* **9,** 647–657
2. Cuervo, A., and Carrascosa, J. L. (2012) Viral connectors for DNA encapsulation. *Curr. Opin. Biotechnol.* **23,** 529–536
3. Tavares, P., Zinn-Justin, S., and Orlova, E. V. (2012) Genome gating in tailed bacteriophage capsids. *Adv. Exp. Med. Biol.* **726,** 585–600
4. Ackermann, H. W. (2007) 5500 phages examined in the electron microscope. *Arch. Virol.* **152,** 227–243
5. Cuervo, A., and Carrascosa, J. L. (2012) *Bacteriophages: Structure*, pp. 1–7, John Wiley & Sons, Ltd., Chichester, UK
6. Casjens, S. R., and Molineux, I. J. (2012) Short noncontractile tail machines: adsorption and DNA delivery by podoviruses. *Adv. Exp. Med. Biol.* **726,** 143–179
7. Xiang, Y., Morais, M. C., Battisti, A. J., Grimes, S., Jardine, P. J., Anderson, D. L., and Rossmann, M. G. (2006) Structural changes of bacteriophage ϕ29 upon DNA packaging and release. *EMBO J.* **25,** 5229–5239
8. Lander, G. C., Tang, L., Casjens, S. R., Gilcrease, E. B., Prevelige, P., Poliakov, A., Potter, C. S., Carragher, B., and Johnson, J. E. (2006) The structure of an infectious P22 virion shows the signal for headful DNA packaging. *Science* **312,** 1791–1795
9. Liu, X., Zhang, Q., Murata, K., Baker, M. L., Sullivan, M. B., Fu, C., Dougherty, M. T., Schmid, M. F., Osburne, M. S., Chisholm, S. W., and Chiu, W. (2010) Structural changes in a marine podovirus associated with release of its genome into *Prochlorococcus*. *Nat. Struct. Mol. Biol.* **17,** 830–836
10. Choi, K. H., McPartland, J., Kaganman, I., Bowman, V. D., Rothman-Denes, L. B., and Rossmann, M. G. (2008) Insight into DNA and protein transport in double-stranded DNA viruses: the structure of bacteriophage N4. *J. Mol. Biol.* **378,** 726–736
11. Jiang, W., Chang, J., Jakana, J., Weigele, P., King, J., and Chiu, W. (2006) Structure of ϵ15 bacteriophage reveals genome organization and DNA packaging/injection apparatus. *Nature* **439,** 612–616
12. Leiman, P. G., Battisti, A. J., Bowman, V. D., Stummeyer, K., Mühlenhoff, M., Gerardy-Schahn, R., Scholl, D., and Molineux, I. J. (2007) The structures of bacteriophages K1E and K1–5 explain processive degradation of polysaccharide capsules and evolution of new host specificities. *J. Mol. Biol.* **371,** 836–849
13. Olia, A. S., Prevelige, P. E., Jr., Johnson, J. E., and Cingolani, G. (2011) Three-dimensional structure of a viral genome-delivery portal vertex. *Nat. Struct. Mol. Biol.* **18,** 597–603
14. Kemp, P., Garcia, L. R., and Molineux, I. J. (2005) Changes in bacteriophage T7 virion structure at the initiation of infection. *Virology* **340,** 307–317
15. Hu, B., Margolin, W., Molineux, I. J., and Liu, J. (2013) The bacteriophage t7 virion undergoes extensive structural remodeling during infection. *Science* **339,** 576–579
16. Agirrezabala, X., Martín-Benito, J., Castón, J. R., Miranda, R., Valpuesta, J. M., and Carrascosa, J. L. (2005) Maturation of phage T7 involves structural modification of both shell and inner core components. *EMBO J.* **24,** 3820–3829
17. Serwer, P., and Jiang, W. (2012) Dualities in the analysis of phage DNA packaging motors. *Bacteriophage* **2,** 239–255
18. Agirrezabala, X., Martín-Benito, J., Valle, M., González, J. M., Valencia, A., Valpuesta, J. M., and Carrascosa, J. L. (2005) Structure of the connector of bacteriophage T7 at 8 Å resolution: structural homologies of a basic component of a DNA translocating machinery. *J. Mol. Biol.* **347,** 895–902
19. Garcia-Doval, C., and van Raaij, M. J. (2012) Crystallization of the C-terminal domain of the bacteriophage T7 fibre protein gp17. *Acta Crystallogr. Sect. F Struct. Biol. Cryst. Commun.* **68,** 166–171
20. Steven, A. C., Trus, B. L., Maizel, J. V., Unser, M., Parry, D. A., Wall, J. S., Hainfeld, J. F., and Studier, F. W. (1988) Molecular substructure of a viral receptor-recognition protein. The gp17 tail-fiber of bacteriophage T7. *J. Mol. Biol.* **200,** 351–365
21. Garcia-Doval, C., and van Raaij, M. J. (2012) Structure of the receptor-binding carboxyl-terminal domain of bacteriophage T7 tail fibers. *Proc. Natl. Acad. Sci. U.S.A.* **109,** 9390–9395
22. Fumagalli, L., Esteban-Ferrer, D., Cuervo, A., Carrascosa, J. L., and Gomila, G. (2012) Label-free identification of single dielectric nanoparticles and viruses with ultraweak polarization forces. *Nat. Mater.* **11,** 808–816
23. Sambrook, J., Fritsch, E. F., and Maniatis, T. (1989) *Molecular Cloning: A Laboratory Manual,* pp. 74–76, Cold Spring Harbor Laboratory Press, Cold Spring Harbor, N.Y.
24. Daudén, M. I., Martín-Benito, J., Sánchez-Ferrero, J. C., Pulido-Cid, M., Valpuesta, J. M., and Carrascosa, J. L. (2013) Large terminase conformational change induced by connector binding in bacteriophage T7. *J. Biol. Chem.* **288,** 16998–17007
25. Scheres, S. H., Núñez-Ramírez, R., Sorzano, C. O., Carazo, J. M., and Marabini, R. (2008) Image processing for electron microscopy single-particle analysis using XMIPP. *Nat. Protoc.* **3,** 977–990

26. Sorzano, C. O., Marabini, R., Velázquez-Muriel, J., Bilbao-Castro, J. R., Scheres, S. H., Carazo, J. M., and Pascual-Montano, A. (2004) XMIPP: a new generation of an open-source image processing package for electron microscopy. *J. Struct. Biol.* **148,** 194–204
27. Sorzano, C. O., Bilbao-Castro, J. R., Shkolnisky, Y., Alcorlo, M., Melero, R., Caffarena-Fernández, G., Li, M., Xu, G., Marabini, R., and Carazo, J. M. (2010) A clustering approach to multireference alignment of single-particle projections in electron microscopy. *J. Struct. Biol.* **171,** 197–206
28. Ludtke, S. J., Baldwin, P. R., and Chiu, W. (1999) EMAN: semiautomated software for high-resolution single-particle reconstructions. *J. Struct. Biol.* **128,** 82–97
29. Scheres, S. H., Valle, M., and Carazo, J. M. (2005) Fast maximum-likelihood refinement of electron microscopy images. *Bioinformatics* **21,** Suppl. 2, 243–244
30. Frank, J., Radermacher, M., Penczek, P., Zhu, J., Li, Y., Ladjadj, M., and Leith, A. (1996) SPIDER and WEB: processing and visualization of images in 3D electron microscopy and related fields. *J. Struct. Biol.* **116,** 190–199
31. Pettersen, E. F., Goddard, T. D., Huang, C. C., Couch, G. S., Greenblatt, D. M., Meng, E. C., and Ferrin, T. E. (2004) UCSF Chimera–a visualization system for exploratory research and analysis. *J. Comput. Chem.* **25,** 1605–1612
32. Söding, J., Biegert, A., and Lupas, A. N. (2005) The HHpred interactive server for protein homology detection and structure prediction. *Nucleic Acids Res.* **33,** W244–W248
33. Zhang, Y. (2008) I-TASSER server for protein 3D structure prediction. *BMC Bioinformatics* **9,** 40
34. Hunter, S., Jones, P., Mitchell, A., Apweiler, R., Attwood, T. K., Bateman, A., Bernard, T., Binns, D., Bork, P., Burge, S., de Castro, E., Coggill, P., Corbett, M., Das, U., Daugherty, L., Duquenne, L., Finn, R. D., Fraser, M., Gough, J., Haft, D., Hulo, N., Kahn, D., Kelly, E., Letunic, I., Lonsdale, D., Lopez, R., Madera, M., Maslen, J., McAnulla, C., McDowall, J., McMenamin, C., Mi, H., Mutowo-Muellenet, P., Mulder, N., Natale, D., Orengo, C., Pesseat, S., Punta, M., Quinn, A. F., Rivoire, C., Sangrador-Vegas, A., Selengut, J. D., Sigrist, C. J., Scheremetjew, M., Tate, J., Thimmajanarthanan, M., Thomas, P. D., Wu, C. H., Yeats, C., and Yong, S. Y. (2012) InterPro in 2011: new developments in the family and domain prediction database. *Nucleic Acids Res.* **40,** D306–D312
35. Wriggers, W., Milligan, R. A., and McCammon, J. A. (1999) Situs: A package for docking crystal structures into low-resolution maps from electron microscopy. *J. Struct. Biol.* **125,** 185–195
36. Campanacci, V., Veesler, D., Lichière, J., Blangy, S., Sciara, G., Moineau, S., van Sinderen, D., Bron, P., and Cambillau, C. (2010) Solution and electron microscopy characterization of lactococcal phage base plates expressed in *Escherichia coli*. *J. Struct. Biol.* **172,** 75–84
37. Cardarelli, L., Lam, R., Tuite, A., Baker, L. A., Sadowski, P. D., Radford, D. R., Rubinstein, J. L., Battaile, K. P., Chirgadze, N., Maxwell, K. L., and Davidson, A. R. (2010) The crystal structure of bacteriophage HK97 gp6: defining a large family of head-tail connector proteins. *J. Mol. Biol.* **395,** 754–768
38. Olia, A. S., Al-Bassam, J., Winn-Stapley, D. A., Joss, L., Casjens, S. R., and Cingolani, G. (2006) Binding-induced stabilization and assembly of the phage P22 tail accessory factor gp4. *J. Mol. Biol.* **363,** 558–576
39. Lhuillier, S., Gallopin, M., Gilquin, B., Brasilès, S., Lancelot, N., Letellier, G., Gilles, M., Dethan, G., Orlova, E. V., Couprie, J., Tavares, P., and Zinn-Justin, S. (2009) Structure of bacteriophage SPP1 head-to-tail connection reveals mechanism for viral DNA gating. *Proc. Natl. Acad. Sci. U.S.A.* **106,** 8507–8512
40. Veesler, D., and Cambillau, C. (2011) A common evolutionary origin for tailed-bacteriophage functional modules and bacterial machineries. *Microbiol. Mol. Biol. Rev.* **75,** 423–433
41. Tang, J., Lander, G. C., Olia, A. S., Olia, A., Li, R., Casjens, S., Prevelige, P., Jr., Cingolani, G., Baker, T. S., and Johnson, J. E. (2011) Peering down the barrel of a bacteriophage portal: the genome packaging and release valve in P22. *Structure* **19,** 496–502
42. Guasch, A., Pous, J., Ibarra, B., Gomis-Rüth, F. X., Valpuesta, J. M., Sousa, N., Carrascosa, J. L., and Coll, M. (2002) Detailed architecture of a DNA translocating machine: the high-resolution structure of the bacteriophage ϕ29 connector particle. *J. Mol. Biol.* **315,** 663–676
43. Simpson, A. A., Tao, Y., Leiman, P. G., Badasso, M. O., He, Y., Jardine, P. J., Olson, N. H., Morais, M. C., Grimes, S., Anderson, D. L., Baker, T. S., and Rossmann, M. G. (2000) Structure of the bacteriophage ϕ29 DNA packaging motor. *Nature* **408,** 745–750
44. Lebedev, A. A., Krause, M. H., Isidro, A. L., Vagin, A. A., Orlova, E. V., Turner, J., Dodson, E. J., Tavares, P., and Antson, A. A. (2007) Structural framework for DNA translocation via the viral portal protein. *EMBO J.* **26,** 1984–1994
45. Lorenzen, K., Olia, A. S., Uetrecht, C., Cingolani, G., and Heck, A. J. (2008) Determination of stoichiometry and conformational changes in the first step of the P22 tail assembly. *J. Mol. Biol.* **379,** 385–396
46. Olia, A. S., Bhardwaj, A., Joss, L., Casjens, S., and Cingolani, G. (2007) Role of gene 10 protein in the hierarchical assembly of the bacteriophage P22 portal vertex structure. *Biochemistry* **46,** 8776–8784